CRACK IDENTIFICATION APPROACH FOR ROTATING MACHINES BASED ON COMBINATION RESONANCES

Aldemir Ap Cavalini Jr
Leonardo Sanches
Edson Hideki Koroishi
Valder Steffen Jr

Laboratory of Mechanics and Structures (LMEst), National Institute of Mechanics and Structures (INCT – EIE), Federal University of Uberlândia, School of Mechanical Engineering, Av. João Naves de Ávila, 2121, Uberlândia, MG, 38408-196, Brazil, aacjunior@mecanica.ufu.br

Abstract. *In this paper a novel model based crack identification methodology is proposed. The technique uses external applied diagnostic forces at combination resonances frequencies, together with a pseudo-random optimization code known as Differential Evolution. The proposed procedure aims at characterizing the signatures of the crack in the spectral responses of a flexible rotor. The method of Multiple Scales is used to determine the conditions under which combination resonances appear. A finite element model of a rotor composed by a horizontal flexible shaft, two rigid discs, and two ball bearings is used to demonstrate the efficiency of the technique. In this system, the additional excitations are applied by electromagnetic actuators coupled to one of the bearings. The breathing crack is simulated according to the Mayes model, in which the crack transition from fully open to fully close is described by a cosine function. The additional flexibility introduced by the crack is calculated by using the linear fracture mechanics theory. This formulation is interesting since it gives the stiffness matrix of the element containing the crack explicitly in terms of its depth. Random noise is added to the dynamic responses of the rotating machine in order to simulate an experimental environment found in a real plant. Consequently, the robustness of the methodology is tested for adverse conditions.*

Keywords: rotating machines, crack identification, combination resonances, and method of multiple scales.

1. INTRODUCTION

Crack detection techniques based on vibration signals has been an area of intensive research activity in the last three decades as demonstrated by the existence of over 500 papers published on this subject between the 1980s and 1990s (Dimarogonas, 1996). According to Friswell and Penny (2002), most of the developed techniques for beams are based on changes in modal properties, such as natural frequencies, mode shapes, and measured dynamic flexibility. Periodic tests are performed in order to identify deviations from the data of the healthy system. These measures, generally associated with a reliable mathematical model, are then used to estimate the crack location and depth. Sinha et al. (2001), for example, estimated crack location and size in three different beams by minimizing the difference between the measured and predicted natural frequencies by using model updating approaches. However, despite presenting successful results, these techniques prove to be efficient only if the crack depth is severe enough to change significantly the modal properties of the structure, which usually does not happen when incipient cracks are considered. In Salawu (1997), an extended review of research works on crack detection based on changes of natural frequencies can be found.

Concerning rotating machines, there are two widely accepted rules for crack detection in shafts. The first one is based on the monitoring of the synchronous vibration amplitude and phase. According to Bently and Hatch (2002), changes in 1X amplitude and phase are the best primary indicator of crack presence. The second rule relies on 2X vibrations, where the same authors state that if a cracked rotor has a steady unidirectional radial load, then a strong 2X response may appear when the rotor is turning at half of any balance resonance speed. Remember that a cracked shaft produces an anisotropic stiffness, which changes twice per revolution. Using a different approach, Baschschmid et al. (2001) applied a least-squares method based on the frequency domain to identify the location of a crack along a rotor shaft. The crack depth was determined by comparing the static bending moment of the shaft with an identified periodical bending moment, which simulates the crack. Sekhar (2003) proposed a method for on-line identification of cracks in rotors that changes the damage influence in the system by equivalent loads. Forces and moments were applied in the undamaged mathematical model by means of a least-squares method to generate a dynamic behavior identical to the measured one. Kulesza and Sawicki (2009) showed a new model based method where a state observer is designed and an auxiliary single-degree-of-freedom oscillator was used as crack indicator for different possible crack locations along the shaft. The proposed technique was validated numerically and the results proved its capability to detect and locate the crack.

Following a different approach, Mani et al. (2006) proposed a crack detection technique that was numerically applied to a Jeffcott rotor supported by conventional bearings. In this case, the damage was found by applying a

specified diagnostic force on the system by using an electromagnetic actuator (EMA). The presence of the crack led to spectral responses with frequencies at combinations of the rotor speed, its critical speed, and the frequency of the diagnostic force. The multiple scale analysis (MSA) was used to determine the conditions required to create the combinational resonance. Kulesza et al. (2010) and Sawicki et al. (2011) presented successful experimental evaluations using the Mani's approach. The rotor used in their works is composed of a shaft supported by two active magnetic bearings (AMBs) and one disc located at the shaft mid-span. Different diagnostic forces, which were all determined by using MSA, were applied to the shaft by means of one of the AMBs. In the analyses, a small notch was cut by using a wire electric discharge machine close to the disc in order to obtain a behavior similar to the breathing crack mechanism. Despite the satisfactory results, the authors evocate further analytical and experimental investigations of the above diagnostic procedure in order to identify the signatures of the crack presence in the measured spectral responses. Penny and Friswell (2007), who have also investigated numerically the Mani's approach, shared the same point of view. Consequently, the authors suggest that further work is needed to draw a robust condition monitoring technique to determine the presence, location, and severity of a crack from the combination frequencies in the responses, which is the goal of the present contribution. It is worth mentioning that an earlier study of the conveyed technique was performed for cracked beams (Cavalini Jr et al., 2013).

2. CRACKED ROTOR MODEL

Figure 1a presents a rotor segment, represented by a beam element, of length l containing a transverse crack of depth a located at a distance l_A from the node A. The six-degree-of-freedom element is loaded with axial forces, P_1 and P_7, shear forces, P_2, P_3, P_8, and P_9, torsion moments, P_4, and P_{10}, and bending moments, P_5, P_6, P_{11}, and P_{12}. Details about the cross-section of the beam element of diameter D, at the location of the crack, are given in Figure 1b. The cross sectional area without crack is represented by the dashed surface.
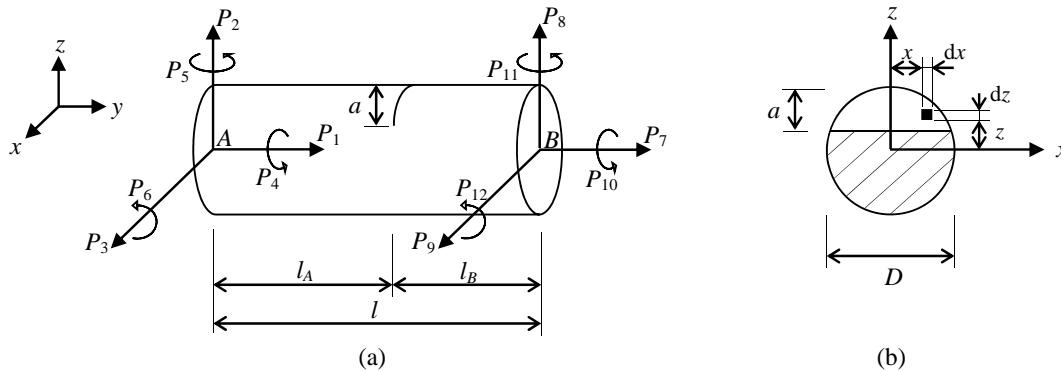

Figure 1. (a) Cracked beam element. (b) Details about the crack element cross-section

Using the Castigliano theorem, the cracked beam displacement u_i in the direction of the load P_i can be determined as shown by Eq. (1), as described by Darpe et al. (2004).

$$u_i = \frac{\partial U_o}{\partial P_i} + \frac{\partial U_c}{\partial P_i} \qquad (1)$$

where U_o is the elastic strain energy of the no-cracked beam element and U_c is the additional strain energy due to the crack presence. The strain energy U_o, that will generate the flexibility finite element matrix of the non-cracked beam, can be derived as described by Imbert (1991).

The concepts of fracture mechanics show that the additional strain energy U_c is given by the integration of the strain energy density function over the crack area A_c (field not hatched in Figure 1b), as given by the Eq. (2).

$$U_c = \frac{1}{E'} \int_{A_c} \left[\left(\sum_{i=1}^{6} K_{Ii} \right)^2 + \left(\sum_{i=1}^{6} K_{IIi} \right)^2 + m \left(\sum_{i=1}^{6} K_{IIIi} \right)^2 \right] dA_c \qquad (2)$$

where $E' = E/(1 - \nu)$ and $m = 1 + \nu$; E is the Young's modulus, ν is the Poisson's ratio, and K_{Ii}, K_{IIi}, and K_{IIIi} are the stress intensification factors corresponding to the opening, sliding, and shear modes of the crack displacement, respectively.

The additional flexibility introduced in the beam element due to the crack presence is obtained with the definition of compliance, as given by Eq. (3):

$$C_{ij} = \frac{\partial^2 U_c}{\partial P_i \partial P_j} \tag{3}$$

where the resulting integrals were calculated by using the procedure described by Papadopoulos and Dimarogonas (1986) and Papadopoulos (2003). Therefore, the additional flexibility matrix due to the crack is:

$$C_c = \begin{bmatrix} C_{11} & 0 & 0 & 0 & C_{15} & C_{16} \\ 0 & 0 & 0 & 0 & 0 & 0 \\ 0 & 0 & 0 & 0 & 0 & 0 \\ 0 & 0 & 0 & C_{44} & 0 & 0 \\ C_{51} & 0 & 0 & 0 & C_{55} & C_{56} \\ C_{61} & 0 & 0 & 0 & C_{65} & C_{66} \end{bmatrix} \tag{4}$$

Considering the crack located at $l_a = l/2$, the flexibility matrix of the cracked element C_{ec} is given by:

$$C_{ec} = B_t^T C_c B_t + C_o \tag{5}$$

where B_t is obtained from the equilibrium conditions of the cracked element (Saavedra and Cuitiño, 2002), and C_o is the flexibility matrix of the no-cracked element (Imbert, 1991).

$$B_t = \begin{bmatrix} -1 & 0 & 0 & 0 & 0 & 0 \\ 0 & -1 & 0 & 0 & 0 & 0 \\ 0 & 0 & -1 & 0 & 0 & 0 \\ 0 & 0 & 0 & -1 & 0 & 0 \\ 0 & 0 & l/2 & 0 & -1 & 0 \\ 0 & -l/2 & 0 & 0 & 0 & -1 \end{bmatrix} \tag{6}$$

The finite element stiffness matrix of the cracked element is determined by considering its equilibrium conditions. Thus, after some algebraic manipulations, the cracked finite element stiffness matrix is found by using Eq. (7).

$$K_{ec} = N C_{ec}^{-1} N^T \tag{7}$$

where N is given by Eq. (8).

$$N = \begin{bmatrix} -1 & 0 & 0 & 0 & 0 & 0 \\ 0 & -1 & 0 & 0 & 0 & 0 \\ 0 & 0 & -1 & 0 & 0 & 0 \\ 0 & 0 & 0 & -1 & 0 & 0 \\ 0 & 0 & l & 0 & -1 & 0 \\ 0 & -l & 0 & 0 & 0 & -1 \\ 1 & 0 & 0 & 0 & 0 & 0 \\ 0 & 1 & 0 & 0 & 0 & 0 \\ 0 & 0 & 1 & 0 & 0 & 0 \\ 0 & 0 & 0 & 1 & 0 & 0 \\ 0 & 0 & 0 & 0 & 1 & 0 \\ 0 & 0 & 0 & 0 & 0 & 1 \end{bmatrix} \tag{8}$$

In this work, the Timoshenko finite element theory is used to model the cracked rotor. Two nodes with four degrees of freedom per node, associated with the shear forces P_2, P_3, P_8, and P_{12} and the bending moments P_5, P_6, P_{11}, and P_{12} are considered. Also, the effects of the sliding and shear modes of the crack displacement are considered negligible ($K_{IIi} = 0$ and $K_{IIIi} = 0$) as compared with the opening effects. Thus, the additional flexibility due to the crack is represented only by C_{55}, C_{56} and C_{66}. Figure 2 shows the behavior of these flexibilities versus the dimensionless crack depth.

The crack breathing law considered follows the model proposed by Mayes and Davies (1976), in which the opening and closing behavior of the crack is weight dominated. Thus, the stiffness of the cracked element changes smoothly according to the cosine of the instantaneous angular position Ωt of the rotating shaft (i.e., fully closed – fully open – fully closed crack transition), as shows the steering function $f(\Omega t)$ defined in Eq. (9).
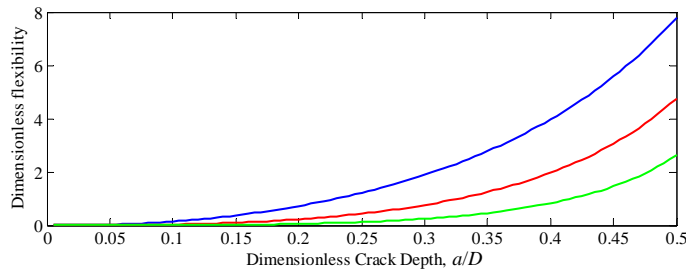
$$f(\Omega t) = \frac{1}{2} \left(1 + \cos(\Omega t) \right) \tag{9}$$

Figure 2. Additional flexibility C_{55} (——), C_{56} (——) and C_{66} (——) versus the dimensionless crack depth

where Ω is the shaft rotation speed and t is the simulation time vector. Penny and Friswell (2007) demonstrate that the Mayes' model can generates, as observed in experimental tests, 1X, 2X, and 3X components in the rotor responses.

Equation 10 presents the equation of motion that governs the dynamic behavior of the cracked flexible rotor supported by roller bearings.

$$[M]\ddot{x} + [D + \Omega D_G]\dot{x} + [K + \dot{\Omega}K_{st}]x = W + F_u + F_s + f(\Omega t)[\Delta K]x \tag{10}$$

where M is the mass matrix, D is the damping matrix, D_G is the gyroscopic matrix, K is the stiffness matrix, and K_{st} is the stiffness matrix resulting from the transient motion. All these matrices are related to the rotating parts of the system, such as couplings, discs, and shaft. W stands for the weight of the rotating parts, F_u represents the unbalance forces, F_s is the vector of the shaft supporting forces produced by the roller bearings, and x is the generalized displacement vector. ΔK represents the maximum stiffness variation due to the crack. Thus, $\Delta K = K - K_{ec}$.

Due to the size of the matrices involved in the equation of motion, the pseudo-modal method is used to reduce the dimension of the finite element model (FE model). For this aim, the reduction is achieved by changing from the physical coordinates x to modal coordinates q, as shows the Eq. (11).

$$x = \phi q \tag{11}$$

where ϕ is the modal matrix containing the *n* first vibration modes of the non-gyroscopic and non-damped system.

Substituting the Eq. (11) into Eq. (10) and multiplying the resulting expression by ϕ^T, the reduced equation of motion of the rotor becomes,

$$[\widetilde{M}]\ddot{q} + [\widetilde{D} + \Omega\widetilde{D}_G]\dot{q} + [\widetilde{K} + \dot{\Omega}\widetilde{K}_{st}]q = \widetilde{W} + \tilde{F}_u + \tilde{F}_s + f(\Omega t)[\Delta\widetilde{K}]q \tag{12}$$

where $\widetilde{M} = \phi^T M \phi$, $\widetilde{D} = \phi^T D \phi$, $\widetilde{D}_G = \phi^T D_G \phi$, $\widetilde{K} = \phi^T K \phi$, $\widetilde{K}_{st} = \phi^T K_{st} \phi$, $\widetilde{W} = \phi^T W$, $\tilde{F}_u = \phi^T F_u$, $\tilde{F}_s = \phi^T F_s$, and $\Delta\widetilde{K} = \phi^T \Delta K \phi$.

The solution of the Eq. (12) results in a response vector described in modal coordinates. By applying the Eq. (11) it is possible to convert the dynamic response to physical coordinates.

3. CRACK IDENTIFICATION

Figure 3 shows a flowchart to illustrate the proposed methodology. The method begins by defining a set of diagnostic forces Ω_{diag} with different combinational frequencies. The frequency of each force is determined by using MSA. According to Mani et al. (2006), the conditions required for a combination resonance occurs when:

$$\Omega_{diag} = |n\Omega - \omega_i| \tag{13}$$

where Ω_{diag} is the frequency of the diagnostic force that will induce the combination resonance, $n = \pm1, \pm2, \pm3, ...,$ (i.e., is the frequency of the external force applied to the structure), and ω_i is a natural frequency of the system.

The determined diagnostic forces are applied to the analyzed system and the corresponding spectral responses are stored (*Original FFTs* - Fast Fourier Transform). The same forces are applied to a reliable finite element model (FE model) of the structure so that the optimizer is responsible for adding the model of a crack with different depths and locations, randomly generated. The obtained spectral responses (*FE model FFTs*) are compared with the original ones by means of a given objective function OF, as shows the Eq. (14). If the procedure converges to a minimum value of the objective function, the crack is identified. If this is not the case, the optimization procedure will propose a new crack configuration (depth and location). The optimization process continues iteratively until convergence is reached.
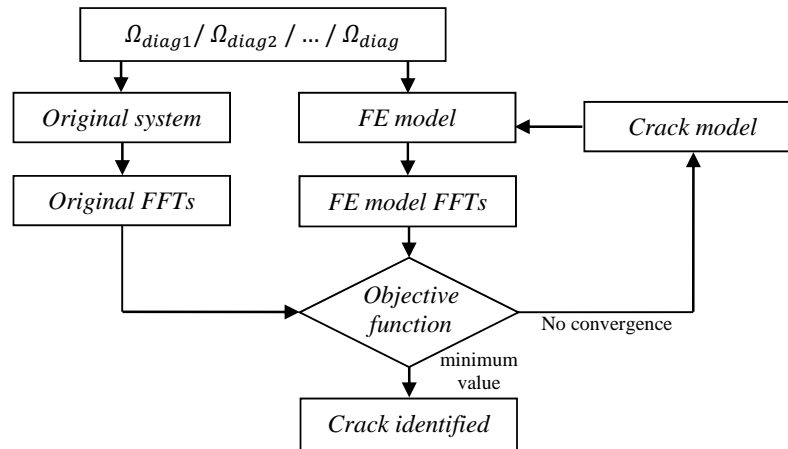
Figure 3. Crack identification flowchart

$$OF = \sum_{j=1}^{s} \frac{\left\| FFT_{orig,j} - FFT_{model,j} \right\|}{\left\| FFT_{orig,j} \right\|} \tag{14}$$

where s is the number of measured spectra, FFT_{orig} stands for the *Original FFTs*, and FFT_{model} represents the *FE model FFTs*. The solution of the inverse problem is performed in this work by using the Differential Evolution algorithm (DE) due to its convergence speed and ability to find a global minimum solution even in the case of complex problems, as proposed by Storn and Price (1995).

4. NUMERICAL APPLICATION

Figure 4 presents the FE model in which 33 finite elements are used to represent the dynamic behavior of the rotor. It is composed of a flexible steel shaft with 860 mm length and 17 mm of diameter (E = 205 GPa, ρ = 7850 kg/m^3, υ = 0.29), two rigid discs D_1 (node #13) and D_2 (node #23), both of steel and with 150 mm of diameter and 20 mm of thickness (ρ = 7850 kg/m^3), and two roller bearings (B_1 and B_2, located at the nodes #4 and #31, respectively). Table 1 summarizes the stiffness and damping parameters of the bearings. The rotating parts take into account a proportional damping ($D = \gamma M + \beta K$) with the coefficients γ = 2.75 and β = 4.85 x 10^{-5}. The effect of the coupling between the electric motor and the shaft was considered by including angular stiffness of 770 N.m/rad around the orthogonal axis (horizontal and vertical directions) at the node #1. In all analyzes that will be shown, the operational spin speed of the rotor Ω is fixed to 1200 rev/min. Figure 5 shows the Campbell diagram of the considered rotor (pristine condition), in which the four first damped natural frequencies at the operational spin speed (backward and forward whirls) are 28.2 Hz, 28.6 Hz, 91.4 Hz, and 97.7 Hz.
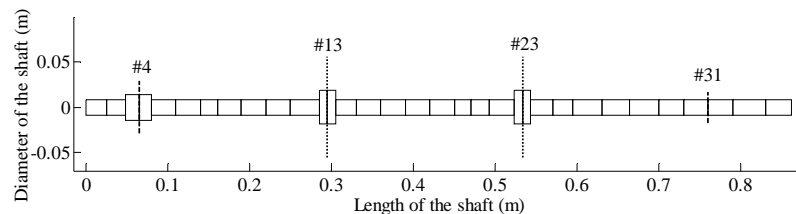

Figure 4. FE model of the rotor (---- Bearing; .... Disc; # node)

Displacement sensors are orthogonally mounted (horizontal and vertical directions) on the nodes #8 and #28 to collect the shaft vibration (the first twelve vibration modes were used to generate the displacement responses). Equation (15) indicates how noise was added to the responses.

$$x_{noise} = x + P \, \text{Rand} \sqrt{E((x - E(x))^2)} \tag{15}$$

where x is the response without noise, x_{noise} is the response with noise, P is the parameter that defines the amount of noise to be added (P = 1% in the present case), and Rand is the random noise. E is the expected value.

Table 1. Stiffness and damping parameters used in the FE model

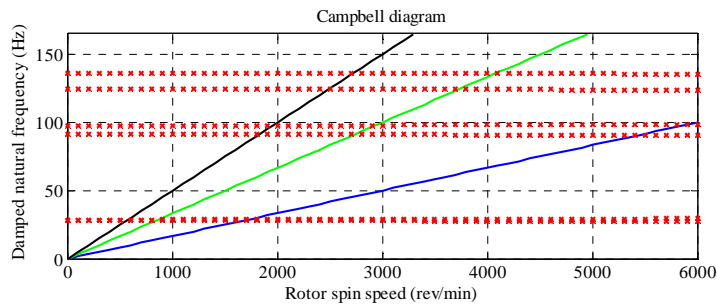| Bearings	Direction	Parameters
B_1	x	$K = 0.85 \; x \; 10^6$ N/m
		$D = 7.45$ Ns/m
	z	$K = 1.20 \; x \; 10^6$ N/m
		$D = 33.7$ Ns/m
B_2	x	$K = 5.20 \; x \; 10^7$ N/m
		$D = 25.58$ Ns/m
	z	$K = 7.02 \; x \; 10^8$ N/m
		$D = 91.03$ Ns/m

Figure 5. Campbell diagram of the simulated rotating machine (—— 1X; —— 2X; —— 3X)

The diagnostic forces are driven on the rotor by two identical EMAs located, along the horizontal direction, at the bearing B_1 (the EMA produces only attractive forces). The EMA model used was constructed according to the approach adopted by Der Hagopian and Mahfoud (2009) and Mahfoud et al. (2010). Based on the magnetic circuit theory and assuming negligible eddy current effects and conservative flux, the relationship between the electromagnetic force and the electric current is given by:

$$F_{EMA} = \frac{N_{coil}\mu_o a \, f \, I^2}{2\left((e \pm \delta) + \dfrac{b + c + d - 2a_e}{\mu_r}\right)^2} \tag{16}$$

where F_{EMA} is the electromagnetic force, N_{coil} is the number of coils, μ_o is the magnetic permeability in the vacuum $(4\pi x 10^{-7} H/m)$, I is the drive current, e is the air gap, δ is the gap distance, and μ_r is the relative dimensionless magnetic permeability; a, b, c, d, and f are the EMA geometric parameters. The properties of the actuators are summarized in Tab. 2.

Table 2. EMA's properties

EMA	Properties
	$a_e = 10$ mm
	$b = 40$ mm
	$c = 30$ mm
	$d = 10$ mm
	$f = 21$ mm
	Effective air gap = 0.5 mm
	Number of Coils = 180
	Relative dimensionless magnetic permeability = 750
	Maximum attraction force: 300 N for 3.0 A

The crack identification methodology was tested for the rotor under three different structural conditions. The first one comprises the shaft without a crack (pristine condition), the second test was performed for the shaft with a crack located at the element #5 (between the nodes #5 and #6) with 30% depth, and the last one corresponds to a crack located

at the element #20, with 30% depth too. Simulations verified that the results were not sensitive to the length of the crack element of 45 mm. Cavalini Jr et al. (2013) previously demonstrated the ability of the methodology for the identification of incipient cracks in beams.

For all the three crack damage conditions, a residual unbalance of 200 g.mm at 0° applied to each disc of the rotor was considered. Under this configuration, the maximum vibration amplitude measured by the sensors reaches 65 µm (peak-to-peak in the operational speed), which is considered as a balanced condition. According to Sinou (2008), the influence of the crack on the nonlinear dynamics of the rotating machine increases when the unbalance magnitude decreases. Also, it is worth mentioning that the unbalance forces must be small enough to allow the weight dominance for the crack breathing, considered by Mayes' model (i.e. static deflection greater than the dynamic response of the rotor).

The frequencies of the diagnostic forces were chosen in order to be distributed along the frequency bandwidth of the four first natural frequencies of the rotor. Thus, using only forward whirl critical speeds (i.e. in steady state motion unbalance forces do not excite the backward whirl), from ω_{fw1} = 28.6 Hz, Ω_{diag} = 48.6, 8.6, 68.6, 11.4, 51.4, and 71.4 Hz. They were obtained, respectively, for n = -1, 1, -2, 2, 4, and 5. Using ω_{fw2} = 97.7 Hz, Ω_{diag} = 77.7, 57.7, 37.7, 17.7, 22.3, and 42.3 Hz. They were obtained, respectively, for n = 1, 2, 3, 4, 6, and 7; giving a total of 12 diagnostic frequencies, resulting in 24 FFTs as only the two sensors along the horizontal direction were used (Ω_{diag} near to the damped natural frequencies and the ones lower than 5 Hz were discarded.). All the diagnostic forces have the same amplitude. Tests were performed for different amplitudes and it was possible to observe that the amplitude has to be changed according to the level of noise. Thus, for the results that will be presented, a satisfactory amplitude value for the diagnostic forces was 25 N.

Figure 6 shows the FFTs obtained using Ω_{diag} = 48.6 Hz for the shaft in its pristine condition, with a 15% depth crack located at the element #20, and a 30% depth crack located at the same element (change in the crack depth only). Note that the amplitudes of the peaks related with each rotor condition are different (i.e. the peaks associated with combination resonances: $\omega_{fw1} - \Omega$, ω_{fw1}, $\omega_{fw1} + 2\Omega$, and so on). Figure 7 shows the FFTs obtained using the same diagnostic force, but for the shaft with a 30% depth crack at the element #5 and a 30% depth crack at the element #20 (change in the crack position along the shaft only). Observe that the peaks associated with the combination resonances also present different amplitudes. For others Ω_{diag}, similar behavior is noted. As mentioned, the proposed methodology uses a set of diagnostic forces with different frequencies to identify cracks. It is possible due to the behavior evidenced by Figs. 6 and 7. The application of several diagnostic forces with different frequencies makes the spectral signature of the crack specific for its characteristic (location and depth), which allows the correct identification. The noise effects associated to the rotor responses were disregarded from these results.
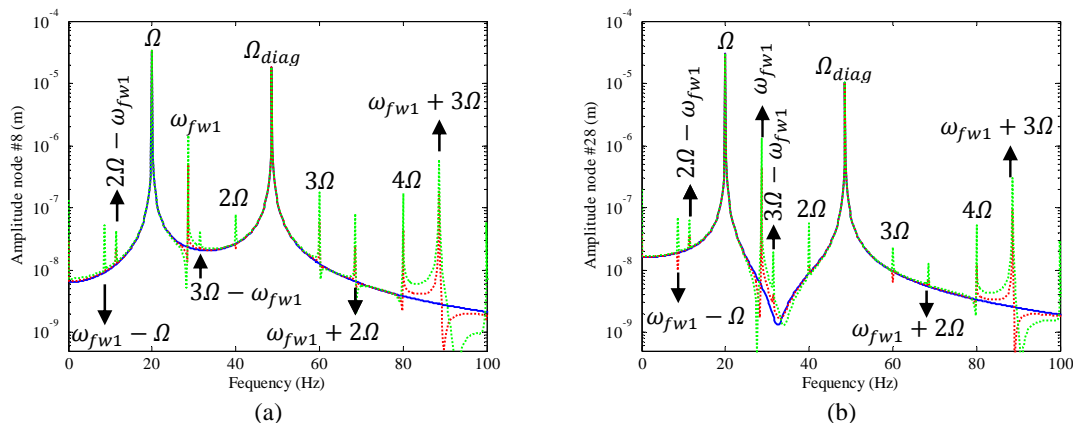

Figure 6. FFTs obtained using Ω_{diag} = 48.6 Hz for the shaft in three structural conditions
(—— pristine; •••• 15% depth crack at element #20; •••• 30% depth crack at element #20)

Table 3 shows the results obtained by the crack identification process. The DE optimizer used 20 individuals in the initial population to identify the structural condition of the rotor. Five optimization processes were carried out for each analysis in order to avoid local minima solutions. The element with crack and the crack depth were used as design variables. Note that the damage configurations were satisfactorily identified. The small differences observed are due to the adverse conditions caused by the noise added to the dynamic responses of the rotor.
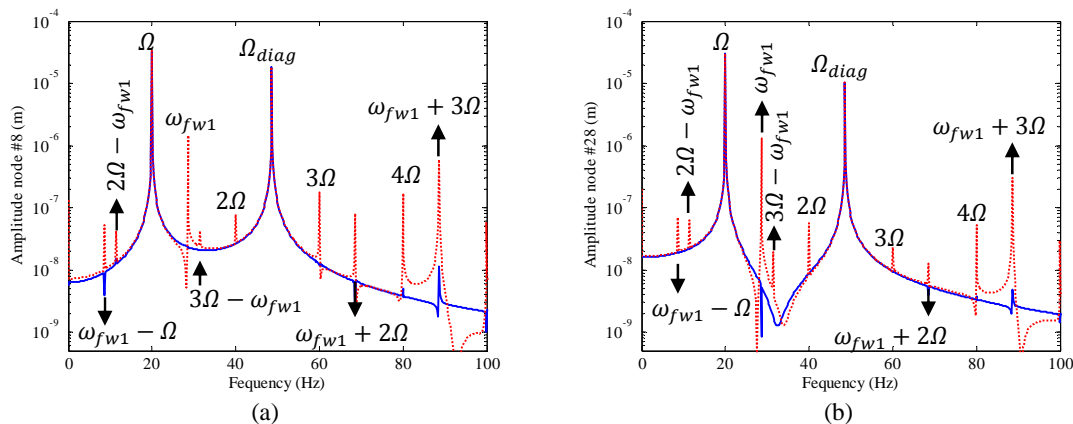
Figure 7. FFTs obtained using $\Omega_{diag} = 48.6$ Hz for the shaft in two structural conditions
(—— 30% depth crack at element #5; •••• 30% depth crack at element #20)

Table 3. Results of the crack identification process

| Structure | Results | |
configuration	Element	Depth (%)
No crack	31	0.08
Element #5 depth 30%	5	31.88
Element #20 depth 30%	20	29.99

Figure 8 compares FFTs obtained from the original system with those found in the end of the identification process for the pristine rotor using the two sensors along the horizontal direction, nodes #8 and #28 (Fig. 8a-8f and Fig 8g-8l, respectively). The goal here was simply to check if the proposed methodology does not lead to false positive alarm. In these FFTs, one can observe only the peaks associated to the excitation frequencies and diagnostic forces, indicating the healthy state of the beam (no extra peaks are found in the spectra). Note that the identification process reproduced satisfactorily the FFTs obtained from the original system and is able to indicate correctly the no-crack condition (see Tab. 2). The remaining FFTs are similar to the previous ones.

Comparing the Fig. 8 and Fig. 9 (nodes #8 and #28 in Fig. 9a-9f and Fig 9g-9l, respectively), one cannot observe different peaks in the spectra as result from the nonlinear effect introduced by the crack presence in the rotor, i.e., the change in the shaft's stiffness (breathing behavior). In this case the rotor has a crack in the element #5 with 30% depth and the optimization process was able to identify satisfactory its location and depth. However, as there is no evidence of diagnostic peaks in the FFTs, the correct identification is addressed with other dynamic effects induced by the crack like changes in 1X vibrations. Note that the crack is located in a region of small strain, which makes the identification harder.

Figure 10 (nodes #8 and #28 in Fig. 10a-10f and Fig 10g-10l, respectively) shows the results of the identification process when the rotor was affected by a crack located in the element #20 with 30% depth. Now, it is possible to observe the diagnostic peaks. Note that the peaks are found for different amplitudes, depending on the frequency of the diagnostic force. The diagnostic peaks show up due to the fact that a deeper crack changes more intensely the dynamic behavior of the beam under the application of the diagnostic forces, i.e., the nonlinear effect becomes more evident in the system responses. It is important to point out that all FFTs are necessary for the success of the crack identification procedure, even those where no extra peaks are found.
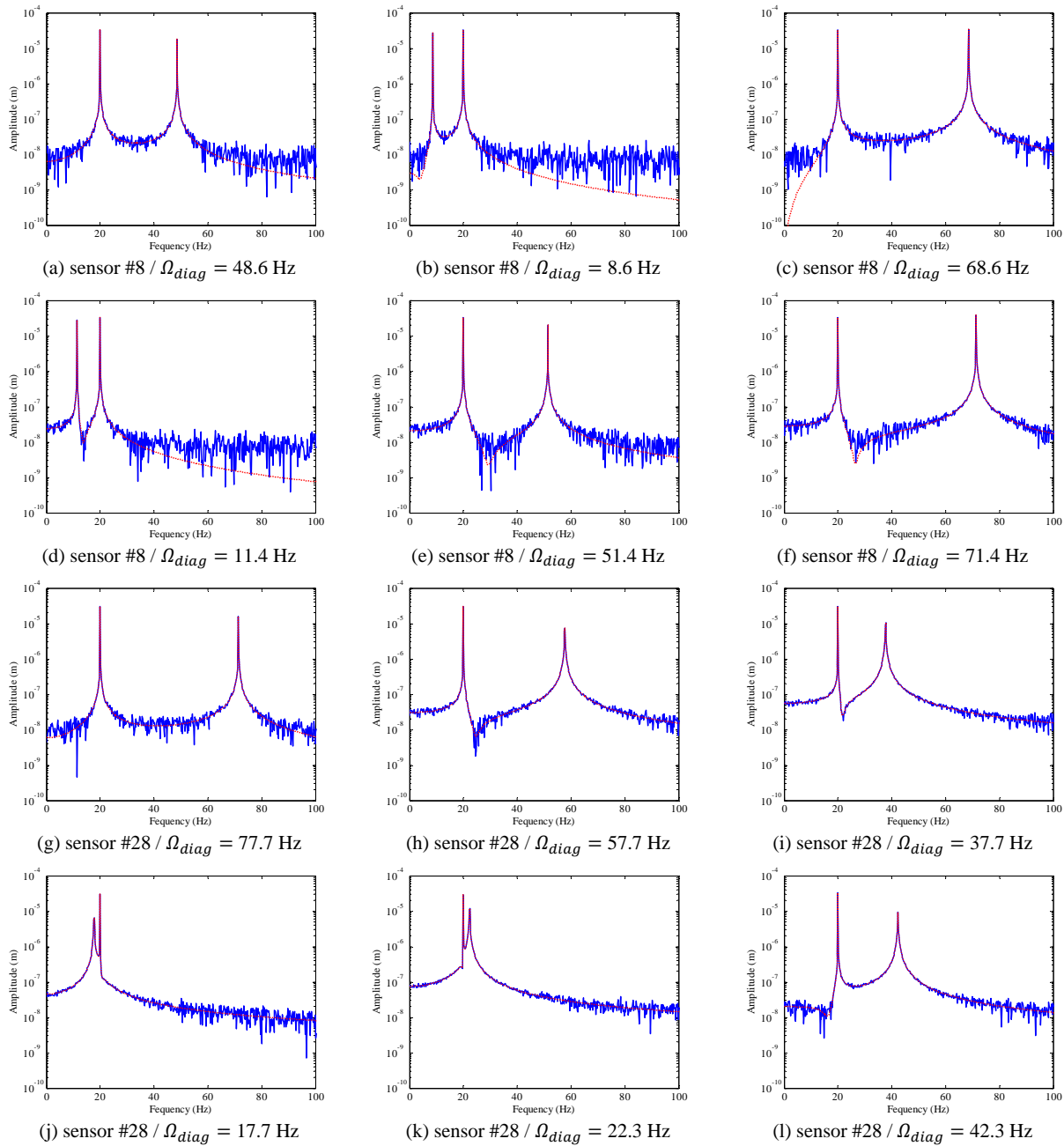
Figure 8. FFTs obtained in the crack identification process; no-crack (—— Original system; .... FE model)

5. CONCLUSIONS

The presented results show that the developed inverse problem methodology is a reliable tool to estimate satisfactorily the existence, location, and depth of a crack. Noise was added to mimic experimental conditions. However, both a representative mathematical model of the mechanical system and the crack breathing mechanism are required (the diagnostic peaks observed in the FFTs depend on the breathing behavior).

It is well known that the crack presence changes the dynamic behavior of the system only for higher frequencies. However, in the proposed methodology this is not a problem since the diagnostic forces generate the diagnostic peaks in the region of the lower vibration modes where the frequency bandwidth is associated with high vibration energy.
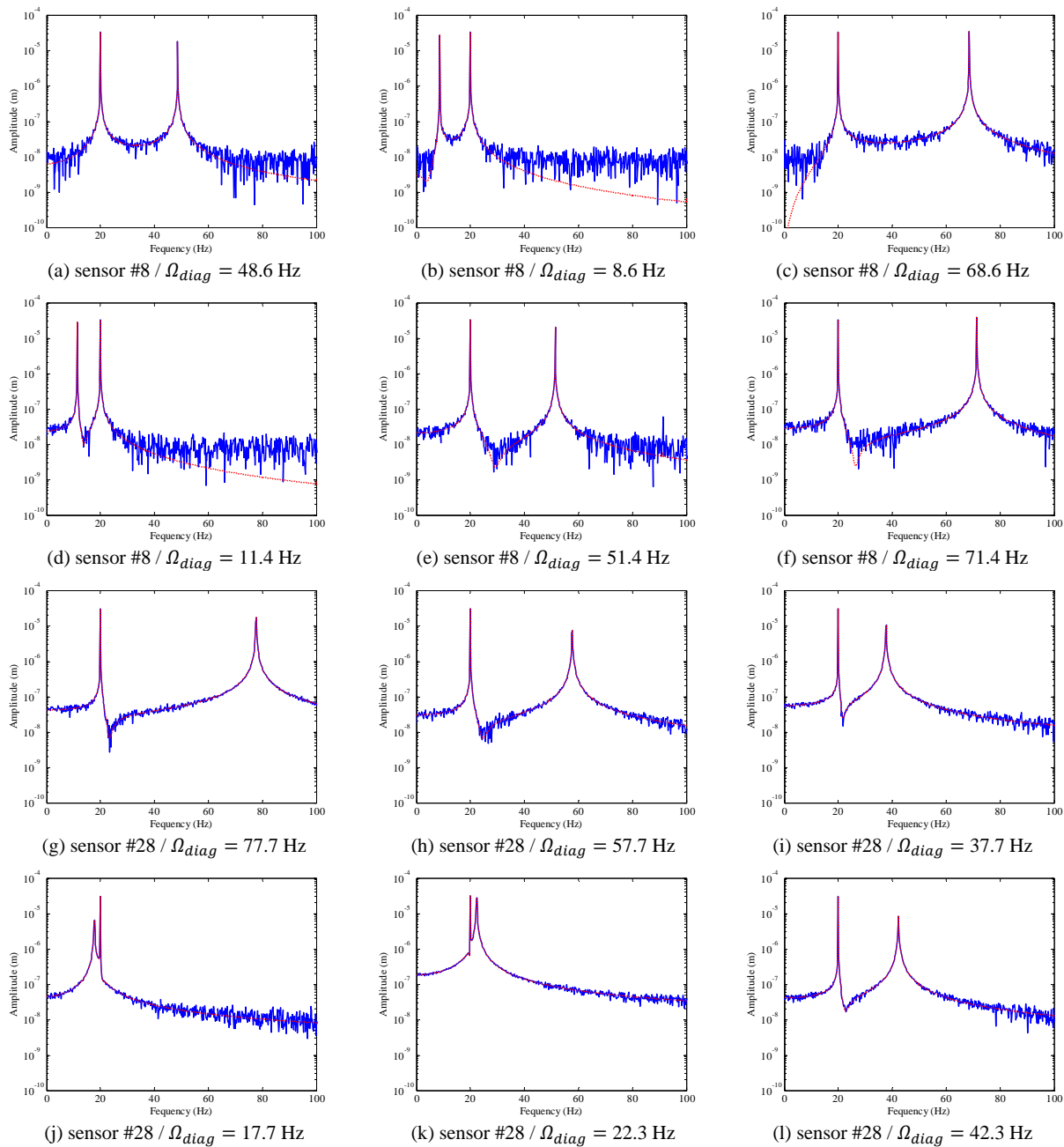
A. A. Cavalini Jr, L. Sanches, E. H. Koroishi, V. Steffen Jr
Crack Identification Approach for Rotating Machines Based on Combination Resonances

Figure 9. FFTs obtained in the crack identification process; element #5 with 30% depth
(—— Original system; **....** FE model)

It is necessary to apply several diagnostic forces to the system to identify the crack. Thus, a time-consuming procedure is expected for the future experimental testing that will be performed. However, in certain cases the diagnostic forces can be applied to the structure under operating conditions. The amplitude of the diagnostic forces can be adjusted to keep the system on a safe vibration level. Additionally, as the amplitude of the diagnostic forces can be adjusted so that difficulties that arise from a faster crack growth due to the effect of adding additional forces to the system can be minimized.

The results presented demonstrate the efficiency and robustness of the methodology conveyed. This encourages further research efforts dedicated to experimental tests for validation purposes.
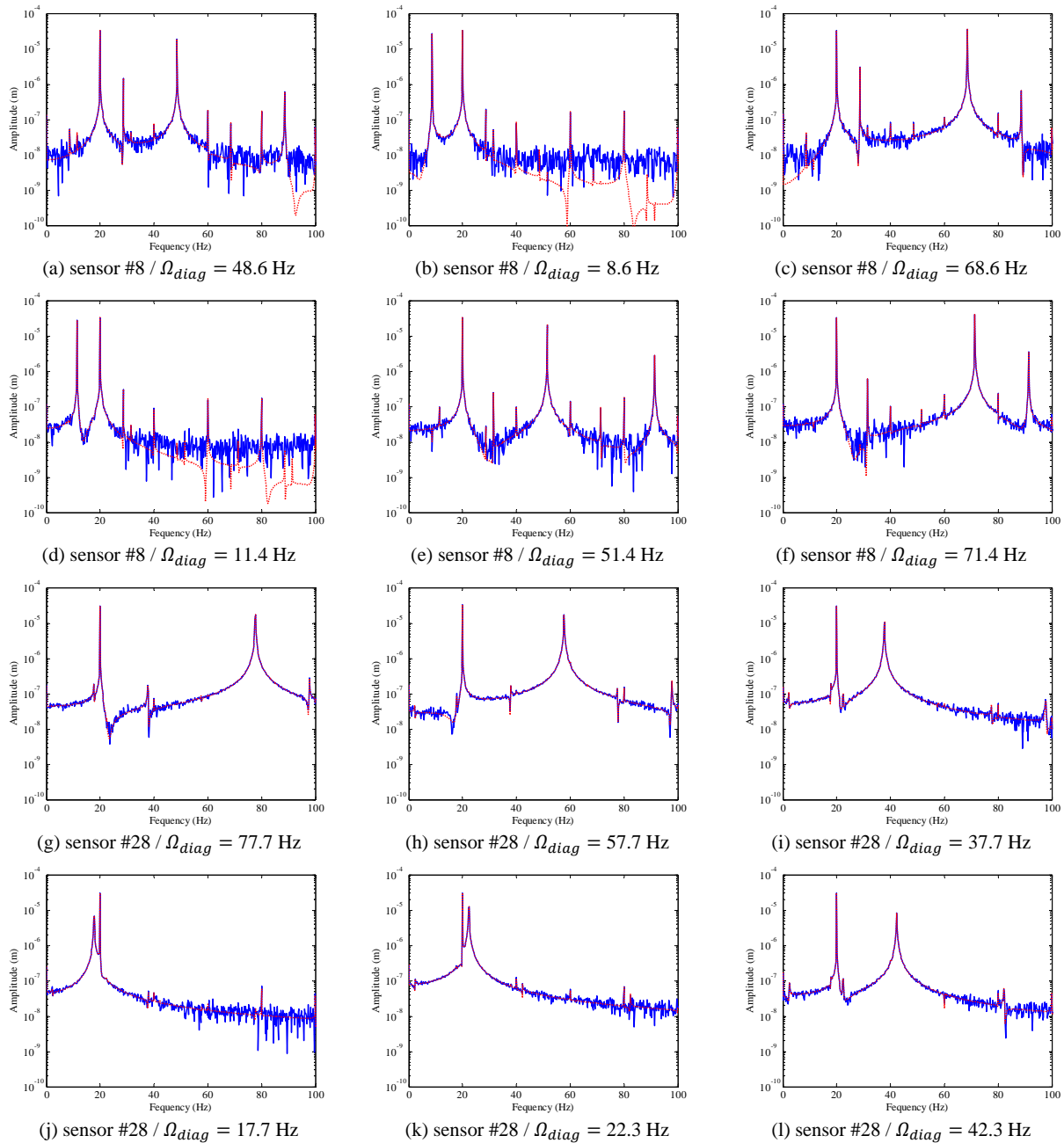
Figure 10. FFTs obtained in the crack identification process; element #20 with 30% depth
(—— Original system; **....** FE model)

(a) sensor #8 / Ω_{diag} = 48.6 Hz
(b) sensor #8 / Ω_{diag} = 8.6 Hz
(c) sensor #8 / Ω_{diag} = 68.6 Hz
(d) sensor #8 / Ω_{diag} = 11.4 Hz
(e) sensor #8 / Ω_{diag} = 51.4 Hz
(f) sensor #8 / Ω_{diag} = 71.4 Hz
(g) sensor #28 / Ω_{diag} = 77.7 Hz
(h) sensor #28 / Ω_{diag} = 57.7 Hz
(i) sensor #28 / Ω_{diag} = 37.7 Hz
(j) sensor #28 / Ω_{diag} = 17.7 Hz
(k) sensor #28 / Ω_{diag} = 22.3 Hz
(l) sensor #28 / Ω_{diag} = 42.3 Hz

6. ACHNOWLEDGEMENTS

7. REFERENCES

Bachschmid, N., Pennacchi, P, Tanzi, E. and Vania, A., 2001, "Identification of Transverse Crack Position and Depth in Rotor Systems", Meccanica, 35, pp. 563-582.
Bently, D.E. and Hatch, C.T., 2002, "Fundamentals of Rotating Machinery Diagnostics", Bently Pressurized Bearing Company, First printing, Minden, NV, USA.

Cavalini Jr, A.A, Steffen Jr, V. and Mafoud, J., 2013, "Crack Identification Approach for a Beam-Like Structure, Proceedings of the XV International Symposium on Dynamic Problems of Mechanics, Buzios, RJ, Brazil.

Darpe, A.K., Gupta, K. and Chawla, A., 2004, "Coupled Bending, Longitudinal and Torsional Vibrations of a Cracked Rotor", Journal of Sound and Vibration, 269 (2004), pp. 33-60.

Der Hagopian, J. and Mahfoud, J., 2009, "Electromagnetic Actuator Design for the Control of Light Structures", Smart Structures and Systems, Vol. 6, No. 1, pp. 29-38.

Dimarogonas, A.D., 1996, "Vibration of Cracked Structures: A State of the Art Review", Engineering Fracture Mechanics, Vol. 55, No. 5, pp. 831-857.

Friswell, M.I. and Penny, J.E.T., 2002, "Crack Modeling for Structure Health Monitoring", Structural Health Monitoring, Vol. 1, No. 2, pp. 139-148.

Imbert, J.F., 1991, "Analyse des Structures par Éléments Finis", Sup'aéro, 504 p.

Kulesza, Z. and Sawicki, J.T., 2009, "Auxiliary State Variables for Rotor Crack Detection", Journal of Vibration and Control, Vol. 17, No. 6, pp. 857-872.

Kulesza, Z., Sawicki, J.T. and Storozhev, D.L., 2010, "Smart Properties of AMB Supported Machines for Rotor Crack Detection: Experimental and Analytical Study", Proceedings of the 8th IFToMM International Conference on Rotordynamics, KIST, Seoul, Korea.

Mahfoud, J., Skladanek, Y. and Der Hagopian, J., 2010, "Active Control and Energy Cost Assessment of a Rotating Machine", Shock and Vibration, 17 (2010), pp. 1-13.

Mani, G., Quinn, D.D. and Kasarda, M., 2006, "Active Health Monitoring in a Rotating Cracked Shaft using Active Magnetic Bearings as Force Actuators", Journal of Sound and Vibration, 294 (2006), pp. 454-465.

Saavedra, P.N. and Cuitiño, L.A., 2002, "Vibration Analysis of Rotor Crack Identification", Journal of Vibration and Control, 8 (2002), pp. 51-57.

Salawu, O.S., 1997, "Detection of Structural Damage Through Changes in Frequencies: A Review", Engineering Structures, Vol. 19, No. 9, pp. 718-723.

Sawicki, J.T., Storozhev, D.L. and Lekki, J.D., 2011, "Exploration of NDE Properties of AMB Supported Rotors for Structural Damage Detection", Journal of Engineering for Gas Turbines and Power, Vol. 133, 9 p.

Sekhar, A.S., 2003, "Crack Identification in a Rotor System: A Model-Based Approach", Journal of Sound and Vibration, 270 (2004), pp. 887-902.

Sinha, J.K., Friswell, M.I. and Edwards, S., 2001, "Simplified Models for the Location of Cracks in Beam Structures Using Measured Vibration Data", Journal of Sound and Vibration, Vol. 251, No. 1, pp. 13-38.

Sinou, J.J., 2008, "Deflection of Cracks in Rotor Based on the 2X and 3X Super-Harmonic Frequency Components and the Crack-Unbalance Interactions", Comunications in Nonlinear Science and Numerical Simulation, Vol. 13, pp. 2024-2040.

Storn, R. and Price, K., 1995, "Differential Evolution: A Simple and Efficient Adaptive Scheme for Global Optimization over Continuous Spaces", International Computer Science Institute, Vol. 12, pp. 1-16.

Papadopoulos, C.A. and Dimarogonas, A.D., 1986, "Coupled Longitudinal and Bending Vibrations of a Rotating Shaft with an Open Crack", Journal of Sound and Vibration, Vol. 117, No. 1, pp. 81-93.

Papadopoulos, C.A., 2003, "Some Comments on the Calculation of the Local Flexibility of Cracked Shafts", Journal of Sound and Vibration, Vol. 278, pp. 1205-1211.

Penny, J.E.T. and Friswell, M.A., 2007, "The Dynamics of Cracked Rotors", Proceedings of the IMAC XXV, Orlando, Florida.

8. RESPONSIBILITY NOTICE

The authors are the only responsible for the printed material included in this paper.